An Adaptive Preprocessing Pipeline for the Enhancement of Camouflaged Lung Tumor Detection in Whole-Body PET-CT Images

N. Shruthi
Department of Information Science and Engineering, JSS Science and Technology University, Mysuru, Karnataka, India
shruthin@jssstuniv.in

N. Manju
Department of Information Science and Engineering, JSS Science and Technology University, Mysuru, Karnataka, India
manjun007@jssstuniv.in (corresponding author)

Received: 10 December 2025 | Revised: 9 January 2026 and 22 January 2026 | Accepted: 2 February 2026

 DOI: https://doi.org/10.48084/etasr.16854

ABSTRACT

Lung cancer is the leading cause of cancer-related mortality worldwide; therefore, its early detection and accurate delineation are important for effective clinical management. A very helpful tool for the diagnosis of lung cancer and its staging is whole-body Positron Emission Tomography Computed Tomography (PET-CT); however, the interpretation of these images is often challenging due to low Signal to Noise Ratios (SNRs), limited contrast, and physiological uptake patterns. As a result, small or low-uptake tumors may become camouflaged within surrounding tissues, potentially delaying diagnosis and increasing uncertainty in clinical decision-making. This study proposes an adaptive image preprocessing framework for whole-body PET-CT to enhance the visibility of camouflaged lung tumors and improve overall image quality for downstream analysis. This framework consists of three self-tuning modules: i) the Adaptive Non-Local Means Denoising (ANLMD), which suppresses noise while preserving structural edges; ii) the Camouflage Aware Contrast Enhancement (CACE), which selectively amplifies low-contrast tumor regions; and iii) the Selective Background Attenuation (SBA), which suppresses physiologically high uptake in non-tumor organs using CT-guided anatomical masking. Contrary to deep-learning-based preprocessing approaches, the proposed approach is fully interpretable, modular, and does not require training or retraining across scanners. Quantitative evaluation revealed significant enhancements in image quality, including a Peak Signal to Noise Ratio (PSNR) of 37.26 dB, a Structural Similarity Index Measure (SSIM) of 0.956, and a Contrast to Noise Ratio (CNR) of 4.55, validating that the proposed methodology produces PET-CT images assisting radiologists for much more accurate interpretation by reducing the camouflage effects and enhancing diagnostic clarity.

Keywords-lung cancer; PET-CT; camouflaged tumors; denoising; contrast enhancement; background attenuation

I. INTRODUCTION

Lung cancer is a leading cause of cancer-related deaths worldwide, representing a large percentage of annual cancer deaths [1]. Early diagnosis and accurate staging of the disease are crucial for patient survival, as the prognosis declines significantly in the advanced stages of the disease. In clinical management, PET-CT has become the imaging modality of choice for lung cancer diagnosis, staging, treatment planning, and therapy response evaluation owing to its ability to combine metabolic information with precise anatomic localization [2].

Despite its clinical importance, reliable tumor visualization on PET-CT remains problematic. This is because the inherently low photon count during PET acquisition yields a poor Signal to Noise Ratio (SNR), while physiological radiotracer uptake in organs, such as the liver, kidneys, myocardium, and bone marrow, frequently produces high-intensity regions that may mimic malignant lesions [3]. Additionally, the intensity patterns of small tumors or lesions with low fluorodeoxyglucose uptake can resemble those of surrounding tissues, thus visually camouflaging tumors to evade detection, even by expert radiologists. This reduces lesion conspicuity, blurs tumor margins, and increases interobserver variability, which affects diagnostic confidence and the accuracy of treatment planning [4].

Various traditional preprocessing techniques have been employed to enhance the visual quality of PET-CT imaging, including Gaussian and median filtering, global Histogram Equalization (HE), and fixed threshold background suppression [5]. However, these methods rely on static parameters and local operations that often over-smooth lesion boundaries, suppress diagnostically relevant uptake, or amplify noise in low-count regions. Consequently, camouflaged tumors, particularly in anatomically complex regions, such as the lung mediastinum or lung liver interface, may remain inadequately visualized [6].

More advanced denoising approaches, such as Non-Local Means (NLM) filtering and its PET-adapted variants, aim to reduce noise while preserving structural details [7]. Nevertheless, classical NLM methods are highly sensitive to parameter selection and perform inconsistently under spatially varying noise conditions that are commonly observed in PET images [8]. Deep-learning-based denoising and reconstruction methods, including Convolutional Neural Networks (CNNs) and diffusion probabilistic models, have demonstrated strong quantitative performance in terms of PSNR and SSIM. However, such methods require large training sets specific to each scanner and often fail to generalize well from one acquisition protocol to another, thereby decreasing their reliability in clinical settings [9-12].

Beyond noise reduction techniques, contrast enhancement is an important step towards separating tumors from the surrounding tissues [13]. Traditional techniques, including HE, Contrast Limited Adaptive Histogram Equalization (CLAHE), and gamma correction, can globally increase the contrast, but they often accentuate the noise and physiological uptake of the PET modality [14]. More recent adaptive algorithms have attempted to focus on metabolically active regions; however, they often do not provide anatomical mapping, and tumors are often difficult to distinguish from the surrounding tissues.

The other significant challenge associated with the preprocessing of PET-CT images is managing the effect of background attenuation and suppressing false-positive information. These issues associated with thresholding algorithms, such as Volume and Contrast Adjusted Thresholding (VCAT) and probabilistic tumor and background algorithms, tend to be very dependent on Standardized Uptake Values (SUV) and tumor heterogeneity [15, 16]. The combination of PET and CT information to take advantage of the anatomical information available from the CT images associated with high uptake values and lesion separations has shown promise, but is often linked to specific preprocessing pathways [17].

Advances in deep-learning-based PET-CT segmentation, such as U-Net architectures and adaptive frameworks like no-new-Net (nnU-Net), have demonstrated strong performance when high-quality inputs are available. However, the performance is dependent on the image processing output and diminishes when there is less contrast or when camouflaging is present in the lesion [18-23]. Previous studies on automated lesion delineation in PET imaging have also highlighted the limitations of threshold-based and semi-automatic methods, particularly in low-contrast regions where boundary uncertainty remains high [24]. These findings underscore the importance of preprocessing techniques that enhance lesion contrast while preserving structural integrity prior to segmentation.

Adaptive preprocessing strategies using multi-annotator learning frameworks, which have shown improved robustness in lung lesion segmentation under heterogeneous imaging conditions, have been explored [25]. Hybrid Artificial Intelligence (AI) models combining CNNs with traditional machine learning classifiers have demonstrated promising performance in lung cancer detection tasks, offering a more interpretable alternative to purely deep-learning-based solutions [26]. Additional research has focused on improving PET image quality through multimodal fusion and advanced modeling techniques. Anatomically and metabolically informed diffusion models have been proposed to enhance lesion visibility in low-count PET acquisitions [27], while radiomics-based approaches incorporating intratumoral and peritumoral PET-CT features have shown potential in predicting immunotherapy response in Non-Small Cell Lung Cancer (NSCLC) [28]. Moreover, integrative radiogenomics frameworks, combining PET radiomics and clinical variables, have shown improved prognostic stratification capabilities [29]. Finally, deep multimodal fusion techniques and AI-based image enhancement methods for PET and Single-Photon Emission Computed Tomography (SPECT) imaging have also contributed to improved diagnostic and segmentation performance [30, 31].

These studies (Table I) demonstrate that preprocessing, multimodal fusion, and hybrid intelligence frameworks play a critical role in improving segmentation accuracy and clinical interpretability. Nevertheless, most existing approaches address denoising, contrast enhancement, or background suppression in isolation, often relying on fixed parameters or data-intensive learning models. A unified, interpretable, and adaptive preprocessing framework that explicitly targets tumor camouflage in whole-body PET-CT imaging, while remaining independent of downstream segmentation architectures, remains underexplored.

Motivated by these gaps, the present study proposes an adaptive preprocessing pipeline to enhance the visibility of camouflaged lung tumors in whole-body PET-CT images. The framework integrates three self-tuning modules: i) the ANLMD for scan-specific noise suppression with edge preservation, ii) the CACE for selective amplification of low contrast tumor regions, and iii) the SBA for CT-guided suppression of physiologically high-uptake structures.

In contrast to the learning-based preprocessing methods summarized in Table I, which require scanner-specific training, fixed data distributions, and limited interpretability, the proposed framework directly addresses tumor camouflage through a scan-adaptive, self-tuning, and fully interpretable design that operates independently of model training. Unlike fixed parameter filters (e.g., Gaussian and Median) or data-intensive deep learning denoisers, this method adapts to scan-specific uptake characteristics. Furthermore, the proposed technique is a lightweight, modular, and clinically feasible solution that fills the gap between traditional preprocessing and black-box AI approaches.

TABLE I. SUMMARY OF EXISTING PREPROCESSING METHODS AND LIMITATIONS

Category	Existing approaches	Limitations
Denoising	Gaussian, Median, Bilateral filters [5], NLM [7], and deep-learning-based denoisers (CNN [9], Denoising Diffusion Probabilistic Model (DDPM) [10]).	Traditional filters often blur the boundaries of tumors, leading to the loss of fine details of lesions [5]. The NLM is highly sensitive to acquisition noise and the choice of parameters, which reduces the consistency between scans [7]. Training deep learning denoisers requires dataset-specific data and limits their generalization to unseen cohorts [9-11].
Contrast enhancement	HE, Gamma correction [5], CLAHE [14].	HE and gamma correction tend to over-amplify noise in low SNR PET regions, degrading image reliability [5]. CLAHE may exaggerate physiological uptake [14].
Background attenuation	Otsu thresholding [15], VCAT [16], and tumor-background likelihood models [17].	Poor robustness under low contrast conditions [15]. Thresholding is SUV dependent and sensitive to heterogeneity [16, 17].

The main contributions of this study are:

- A unified adaptive preprocessing pipeline for whole-body PET-CT imaging that jointly addresses noise suppression, tumor camouflage, and background attenuation within a single-scan specific framework.
- A camouflage-aware contrast enhancement strategy that selectively improves lesion conspicuity in low-gradient regions while preserving anatomical boundaries using CT-guided edge information.
- An SBA mechanism that leverages semi-automatic CT-derived organ masking to suppress physiologically high uptake without compromising tumor integrity.
- A comprehensive validation of The Cancer Imaging Archive (TCIA) NSCLC radiogenomics dataset using standard image quality metrics, including PSNR, SSIM, and CNR, and blinded radiologist assessment.

II. METHODOLOGY

A. System Architecture

The proposed framework works on PET-CT images, which are processed through a series of operations to make tumor visibility more prominent, as depicted in Figure 1. Initially, the image intensities are normalized to allow for fair comparison. Subsequently, an adaptive processing scheme is applied to denoise, enhance contrast, and remove background activity. This adaptive processing is tuned to each scan, thereby enhancing lesion conspicuity while preparing the images for segmentation.

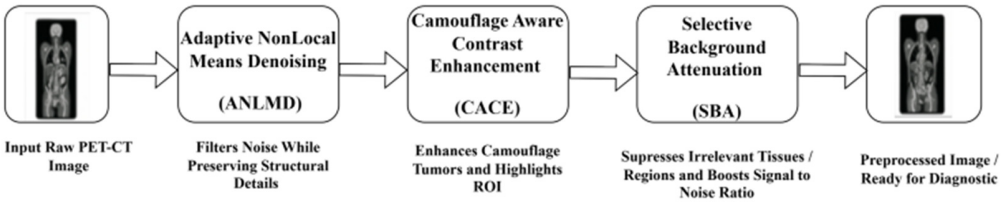

Fig. 1. Architecture of the proposed adaptive preprocessing pipeline.

B. Dataset Description

The imaging data used in this study were retrieved from the Fluorodeoxyglucose Positron Emission Tomography Computed Tomography (FDG-PET-CT)-lesions collection of the TCIA database [32]. This publicly accessible database comprises 1,014 whole-body FDG-PET-CT scans, of which 501 contain FDG-avid malignant lesions across various cancer types. For this study, only the PET-CT scans with histopathologically proven NSCLC were used.

Selection was performed using the clinical metadata available in TCIA, yielding 120 patient-level NSCLC PET-CT scans. Eight scans were excluded based on quality control criteria, including five with severe respiratory motion artifacts and three with incomplete metadata or missing imaging modalities. Consequently, 112 whole-body NSCLC PET-CT scans were included in the final analysis. All PET-CT images were retained in SUV units. Additionally, no lesion-level cropping or manual masking was performed, ensuring that the proposed preprocessing pipeline operates on full whole-body scans under realistic clinical conditions.

Furthermore, camouflaged tumors were operationally defined as lesions with low tumor-to-background contrast, quantified as SUV contrast within one standard deviation of the surrounding tissue uptake, and exhibiting indistinct or visually ambiguous boundaries on PET images, particularly near regions of physiological uptake. This definition corresponds directly to the contrast-based analysis performed using CNR. All candidate camouflaged lesions were confirmed by visual assessment by an experienced imaging researcher to ensure consistency across the dataset. The dataset was used in accordance with TCIA data usage policies.

C. Implementation of the Adaptive Preprocessing Pipeline

The proposed pipeline consists of three sequential modules, ANLMD, CACE, and SBA.

1) Adaptive Non-Local Means Denoising Module

The ANLMD module refines the PET images by reducing the noise while preserving the structural details. It extends the classical NLM algorithm with adaptive weighting to handle

spatial variations in noise and anatomical structures. The steps of this approach are:

a) Step 1: Patch-based Similarity and Adaptive Weighting

Patch-based similarity is computed for each voxel, and adaptive weights are assigned to prevent over-smoothing of tumor regions, ensuring preservation of rare tumor-like voxels.

b) Step 2: Edge-Aware Modulation

To avoid blurring across anatomical boundaries, the weights are further adjusted using CT-derived edge information.

c) Step 3: Denoised PET Intensity

The final denoised intensity is obtained by normalized weighted averaging using (1), which produces an adaptively smoothed PET image and preserves the lesion boundaries:

$$\hat{I}_{PET}(x) = \sum_{y\epsilon\Omega} w_e(x,y) I_{PET}(y) \quad (1)$$

where $\hat{I}_{PET}(x)$ is the denoised PET intensity at the voxel x, $I_{PET}(y)$ is the original PET intensity at the neighboring voxel y, and Ω searches the neighbourhood centered at the voxel x.

Figure 2(a) shows the original image of the PET-CT image, and Figure 2(b) displays the ANLMD-denoised result. The output demonstrates a distinct reduction in background noise while maintaining sharp tumor boundaries and fine anatomical structures when compared to the raw input, providing a reliable basis for subsequent contrast enhancement.

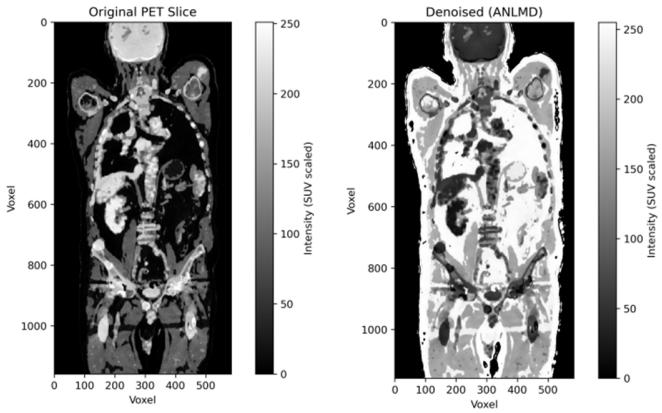

(a) (b)

Fig. 2. (a) Original PET-CT image, (b) ANLMD denoised image.

2) Camouflage Aware Contrast Enhancement Module

CACE selectively enhances tumor regions with low visual separability from the surrounding tissue after ANLMD denoising. The conventional approach, using global contrast stretching, tends to amplify noise and physiologically high uptake regions, such as the liver and kidneys, which can reduce segmentation accuracy. In contrast, the proposed CACE module is designed to adaptively modulate the enhancement strength according to local rarity, lesion probability, and structural edges, while simultaneously attenuating background uptake. The procedure involves the following steps:

a) Step 1: Z-Score Normalization

The PET volume $I_{PET}(x)$ is normalized using z-score normalization with respect to the Interquartile Range (IQR):

$$I_N(x) = \frac{I_{PET}(x) - \mu_{IQR}}{\sigma_{IQR}} \quad (2)$$

where $I_N(x)$ is the normalized PET intensity, $I_{PET}(x)$ is the original PET SUV value at the voxel x, μ_{IQR} is the median intensity, and σ_{IQR} is the scale parameter derived from the IQR, which reduces sensitivity to extreme uptake values.

b) Step 2: Local Rarity Measure

Local rarity $C(x)$ is computed to estimate tumor camouflage likelihood:

$$C(x) = \alpha I_N(x) + \beta \frac{|I_N(x) - \mu_N(x)|}{\sigma_N(x) + \varepsilon} \quad (3)$$

where α and β are weighting coefficients controlling the contribution of absolute intensity and local rarity, respectively, while $\mu_N(x)$ and $\sigma_N(x)$ are the local mean and standard deviation, and ε is a small constant to prevent numerical instability. A sigmoid function is then applied to emphasize camouflaged regions, and the resulting map is refined using CT edge information:

$$C'(x) = \frac{1}{1 + \exp\left([-\lambda(C(x) - \tau)]\right)} \quad (4)$$

where $C'(x)$ is the nonlinearly enhanced camouflage response, λ is the slope parameter controlling emphasis strength, and τ is the activation threshold.

c) Step 3: Region Aware Tone Mapping

The PET intensities are adjusted based on the refined camouflage map, using:

$$I_E(x) = [I_N(x)]^{\gamma(x)}$$

$$\gamma(x) = \gamma_{\max} - C_s(x)(\gamma_{\max} - \gamma_{\min}) \quad (5)$$

where $I_E(x)$ is the enhanced PET intensity, $\gamma(x)$ is the spatially adaptive gamma parameter, $\gamma_{\max}$ is the upper and $\gamma_{\min}$ is the lower bound for gamma correction, and $C_s(x)$is the smoothed and edge-refined camouflage probability derived from $C'(x)$.

d) Step 4: Edge Preserving Blending

The enhanced image was blended with the original PET volume according to:

$$I_{CACE}(x) = Rescale((1 - w(x)) I_{PET}(x) + w(x) I_E(x)) \quad (6)$$

where $I_{CACE}(x)$ is the CACE enhanced PET image, $w(x)$ is the blending weight derived from camouflage confidence, and $Rescale()$ is a linear mapping to restore intensities to the clinical SUV range.

Figure 3 illustrates the intermediate outputs of the proposed CACE module. The gradient map highlights the structural boundaries, whereas the variance map (captures regional intensity fluctuations. A low-variance mask is then derived to suppress homogeneous background regions, resulting in the final contrast-enhanced image (with improved lesion visibility and preserved anatomical details).

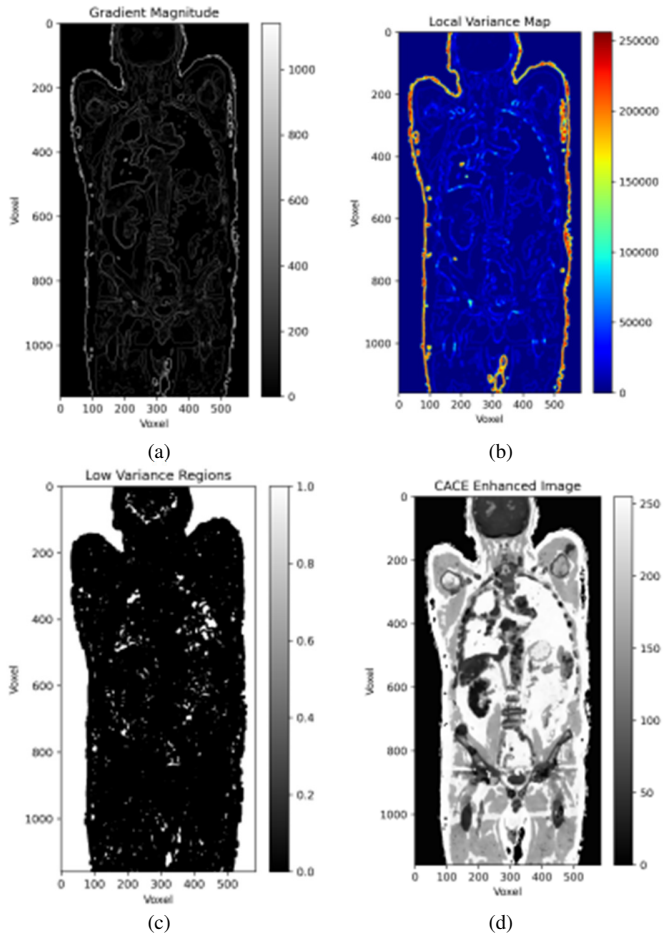

Fig. 3. Intermediate outputs of CACE: (a) gradient map, (b) variance map, (c) low variance mask, and (d) final contrast-enhanced image.

3) Selective Background Attenuation Module

SBA is designed to reduce the visual dominance of non-tumor structures, such as the liver and bones, thereby improving the separability of true lesions from physiologically high-uptake regions. The procedure consists of the following steps:

a) Step 1: Foreground Background Separation

Otsu's threshold method determines the threshold that maximizes the between-class variance. A binary mask $M_{fg}(x)$ is used to differentiate the tumor regions from the background:

$$M_{fg}(x) = \begin{cases} 1, I_{PET}(x) \geq T^* \\ 0, I_{PET}(x) < T^* \end{cases} \quad (7)$$

where $M_{fg}(x)$ is a binary foreground mask indicating potential tumor regions, and T^* is the global threshold obtained using Otsu's method.

b) Step 2: Anatomical Masking of High Uptake Organs

To prevent false positives from physiologically high-uptake regions, anatomical masks were generated from co-registered CT scans. The corresponding background mask is then defined as:

$$M_{bg}(x) = M_{org}(x)[1 - M_{fg}(x)] \quad (8)$$

where $M_{bg}(x)$ is the background mask emphasizing non-tumor structures, and $M_{org}(x)$ is the organ mask derived from CT segmentation (e.g., liver, bone, and heart).

c) Step 3: Selective Logarithmic Compression

For voxels within the background regions, the intensity dominance was suppressed using a logarithmic compression function according to:

$$I_B(x) = \log\left(1 + \alpha I_{PET}(x)\right)$$
$$I_F(x) = \lambda I_{PET}(x) \quad (9)$$

where $I_B(x)$ is the log-compressed background intensity, $I_F(x)$ is the linearly amplified foreground intensity, α is the compression parameter controlling background suppression, and λ is the foreground amplification factor.

d) Step 4: Edge Preserving Blending

Edge-weighted blending was applied to maintain anatomical consistency with the CT gradients and preserve structural integrity, as defined in:

$$I_{SBA}(x) = (1 - \eta E(x))I_B(x) + \eta E(x)I_F(x) \quad (10)$$

where $I_{SBA}(x)$ is the PET image after SBA, $E(x)$ is the edge strength map derived from the CT gradients, and η is the blending coefficient controlling the edge-aware transition between the foreground and background.

e) Step 5: Final SUV Rescaling

The corrected volume was rescaled to the SUV units according to:

$$I_{out}(x) = Rescale(I_{SBA}(x)) \quad (11)$$

where $I_{out}(x)$ is the final preprocessed PET image with preserved SUV fidelity.

Figure 4 displays the effect of the SBA module. Figure 4(a) shows the original PET image after the initial enhancement, where both the tumor regions and physiologically high uptake organs (e.g., liver, kidneys, and bone) appear with similar intensities, making lesion identification difficult. Figure 4(b) presents the automatically derived foreground mask obtained via Otsu's thresholding, which separates probable tumor regions from the background. Finally, Figure 4(c) portrays the background-attenuated image after applying logarithmic compression and edge-preserving blending, where the dominance of non-tumor structures is significantly reduced, whereas true tumor regions are preserved.

III. RESULTS AND DISCUSSION

A. Quantitative Evaluation Metrics

The proposed adaptive preprocessing pipeline was evaluated using three widely accepted image quality metrics, PSNR, SSIM, and CNR.

PSNR is a measure of pixel-level fidelity of the processed image with respect to a reference image. For medical images, a PSNR >40 dB represents an excellent result with no diagnostic loss, a PSNR between 30-40 dB is considered acceptable, and

values <30 dB represent significant degradation. PSNR is computed as:

$$PSNR = 10\log_{10}\left(\frac{MAX_I^2}{MSE}\right) \quad (12)$$

where MAX_I is the maximum possible voxel intensity, and MSE denotes the mean squared error between reference and processed images.

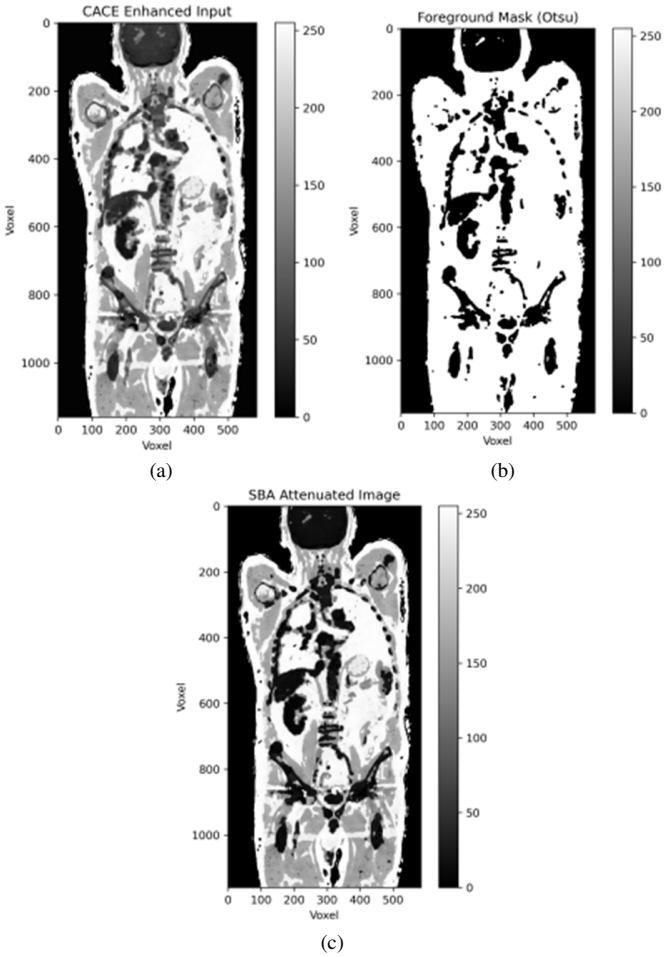

Fig. 4. (a) Original enhanced image, (b) foreground mask, and (c) background attenuated image.

SSIM evaluates perceptual similarity by accounting for luminance, contrast, and structural patterns. It is particularly important in medical imaging to ensure that lesion boundaries and anatomical continuity are preserved after enhancement. SSIM is computed as:

$$SSIM = \frac{(2\mu_x\mu_y+C_1)(2\sigma_{xy}+C_2)}{(\mu_x^2+\mu_y^2+C_1)(\sigma_x^2+\sigma_y^2+C_2)} \quad (13)$$

where $\mu_x\mu_y$ are mean intensities, σ_x^2 and σ_y^2 are variances, σ_{xy} is covariance, while C_1 and C_2 are stabilization constants.

Moreover, the CNR measures lesion conspicuity relative to the surrounding background, with higher values indicating improved detectability. CNR is computed as:

$$CNR = \frac{|\mu_{tumor}-\mu_{background}|}{\sigma_{background}} \quad (14)$$

where μ_{tumor} is the tumor Region of Interest (ROI) mean, $\mu_{background}$ is the background ROI mean, and $\sigma_{background}$ is the background ROI standard deviation.

B. Quantitative Performance of the Proposed Preprocessing Pipeline

The quantitative performance of the proposed preprocessing pipeline at different processing stages is presented in Table II. The ANLMD component significantly improved the image quality, resulting in sharper details and higher fidelity. The PSNR (22.41 dB→36.63 dB) and SSIM (0.68→0.93) values increased significantly, along with an important increase in CNR (1.65→2.52), indicating that the ANLMD suppresses random noise without affecting the crucial details in medical images. Furthermore, the application of CACE enhanced the delineation of lesions, particularly the contrast of tumor regions, resulting in a further increase in CNR (2.52→4.10), even though a minor loss in PSNR (36.63 dB→35.87 dB) was observed owing to contrast enhancement. Finally, SBA achieved the best overall balance among the various approaches studied, which resulted in the maximum PSNR (37.26 dB), SSIM (0.956), and CNR (4.55). The evolution of these metrics throughout the processing stages is also visualized in Figure 5. Overall, the pipeline increased the PSNR by 66.26%, the SSIM by 39.7%, and the CNR by 175.75% compared to the original images. These results indicate that the successive incorporation of ANLMD, CACE, and SBA improved image fidelity, structural preservation, and lesion conspicuity from a clinical perspective and resulted in a clearer PET-CT image suitable for further clinical interpretation and automated analysis.

TABLE II. QUANTITATIVE PERFORMANCE OF THE PROPOSED PREPROCESSING PIPELINE

Processing stage	PSNR (dB)	SSIM	CNR
Input raw PET-CT image (original image)	22.41	0.68	1.65
ANLMD (denoised)	36.63	0.93	2.52
CACE (contrast enhanced)	35.87	0.92	4.10
SBA (proposed adaptive pipeline)	37.26	0.956	4.55

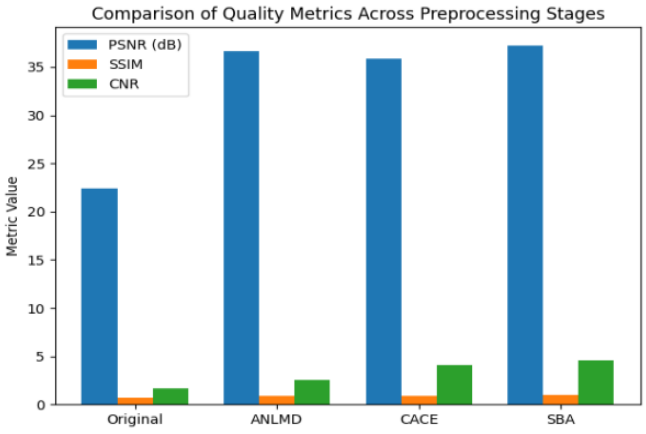

Fig. 5. Comparison of quality metrics across preprocessing stages.

C. Computational Performance and Comparative Evaluation

Experiments were conducted on a standard high-performance workstation equipped with NVIDIA RTX 3080 Ti Graphics Processing Unit (GPU), Intel Core i9-12900K, 32 GB Random Access Memory (RAM), using Python 3.10, PyTorch 2.1, CUDA 12.1, OpenCV 4.8, and SimpleITK 2.3. This configuration was adequate to handle large whole-body PET-CT volumes (512 × 512 × ~300 slices), which require increased memory performance owing to intermediate processing outputs.

Conventional image preprocessing techniques, such as Gaussian filtering [5], have been widely applied to PET-CT enhancement; however, Gaussian filtering tends to oversmooth lesion boundaries. Other methods, such as HE [5], may increase background noise, and CLAHE [14] can amplify noise, particularly in low signal-to-noise PET images. On the other hand, the NLM filter [7] preserves structural details more effectively but has a high computational cost and requires careful parameter tuning. Moreover, DDPM [10] has demonstrated strong denoising performance; however, it requires large training datasets and may compromise interpretability. In contrast, the proposed adaptive preprocessing pipeline is deterministic, does not require model training, and improves lesion conspicuity, as shown in Table III.

TABLE III. COMPARISON OF PREPROCESSING METHODS WITH BASELINE TECHNIQUES

Method	PSNR	SSIM	CNR	Artifact reduction (qualitative)	Run time per slice (ms)
Gaussian filter [5]	Moderate	Low-moderate	Low	Over-smoothing in lung regions.	5-7
HE [5]	Low	Low	High but unstable	Amplifies noise, poor lesion visibility.	2-3
CLAHE [14]	Moderate	Moderate	High	Local contrast improved, but noise amplified.	12-18
NLM [7]	High	High	Moderate	Good detail but very slow; blurs small lesions.	110-150
DDPM-based denoiser [10]	Very high	High	Moderate	Strong restoration but risk of hallucination.	55-70
Proposed adaptive pipeline (ANLMD + CACE + SBA)	High (Best balance)	High	High and stable	Improved lesion conspicuity; suppresses lung background.	27-36

IV. CONCLUSION

This study proposes an adaptive preprocessing framework to enhance the visibility of camouflaged lung tumors in the output of Whole-Body Positron Emission Tomography Computed Tomography (PET-CT) scans. The proposed pipeline technique is composed of three self-tuning modules: Adaptive Non-Local Means Denoising (ANLMD), Camouflage Aware Contrast Enhancement (CACE), and Selective Background Attenuation (SBA). The quantitative evaluation of the proposed pipeline technique was carried out on Non-Small Cell Lung Cancer (NSCLC) patient data, obtained from the Fluorodeoxyglucose Positron Emission Tomography Computed Tomography (FDG-PET-CT)-Lesions collection, by The Cancer Imaging Archive (TCIA), resulting in an improved image quality with a Peak Signal to Noise Ratio (PSNR) of 37.26 dB, a Structural Similarity Index Measure (SSIM) of 0.956, and a Contrast to Noise Ratio (CNR) of 4.55. This indicates that the proposed framework effectively reduces camouflage effects and enhances diagnostic clarity without the need for training or scanner-specific adaptation. While the framework is optimized for lung cancer imaging, extension to other organs may require parameter adjustments due to differing uptake patterns. Future work will focus on multi-cancer validation and integration with multimodal feature analysis to further improve generalizability.

REFERENCES

[1] R. L. Siegel, K. D. Miller, N. S. Wagle, and A. Jemal, "Cancer statistics, 2023," *CA: A Cancer Journal for Clinicians*, vol. 73, no. 1, pp. 17–48, Jan. 2023, https://doi.org/10.3322/caac.21763.

[2] H. AL-Jahdali, A. N. Khan, S. Loutfi, and A. S. Al-Harbi, "Guidelines for the role of FDG-PET/CT in lung cancer management," *Journal of Infection and Public Health*, vol. 5, pp. S35–S40, Dec. 2012, https://doi.org/10.1016/j.jiph.2012.09.003.

[3] J. Qi and R. M. Leahy, "Iterative reconstruction techniques in emission computed tomography," *Physics in Medicine and Biology*, vol. 51, no. 15, pp. R541–R578, Aug. 2006, https://doi.org/10.1088/0031-9155/51/15/R01.

[4] X. Fu, L. Bi, A. Kumar, M. Fulham, and J. Kim, "Multimodal Spatial Attention Module for Targeting Multimodal PET-CT Lung Tumor Segmentation," *IEEE Journal of Biomedical and Health Informatics*, vol. 25, no. 9, pp. 3507–3516, Sept. 2021, https://doi.org/10.1109/JBHI.2021.3059453.

[5] R. C. Gonzalez and R. E. Woods, *Digital image processing*, Fourth, Global edition. New York, New York: Pearson Education, 2018.

[6] K. P. Das and J. Chandra, "A Review on Preprocessing Techniques for Noise Reduction in PET-CT Images for Lung Cancer," in *Congress on Intelligent Systems*, vol. 111, M. Saraswat, H. Sharma, K. Balachandran, J. H. Kim, and J. C. Bansal, Eds. Singapore: Springer Nature Singapore, 2022, pp. 455–475.

[7] A. Buades, B. Coll, and J.-M. Morel, "A Non-Local Algorithm for Image Denoising," in *2005 IEEE Computer Society Conference on Computer Vision and Pattern Recognition (CVPR'05)*, 2005, vol. 2, pp. 60–65, https://doi.org/10.1109/CVPR.2005.38.

[8] J. Cui *et al.*, "PET image denoising using unsupervised deep learning," *European Journal of Nuclear Medicine and Molecular Imaging*, vol. 46, no. 13, pp. 2780–2789, Dec. 2019, https://doi.org/10.1007/s00259-019-04468-4.

[9] Y. Lu, J. Lin, S. Chen, H. He, and Y. Cai, "Automatic Tumor Segmentation by Means of Deep Convolutional U-Net With Pre-Trained Encoder in PET Images," *IEEE Access*, vol. 8, pp. 113636–113648, 2020, https://doi.org/10.1109/ACCESS.2020.3003138.

[10] B. Yu, S. Ozdemir, Y. Dong, W. Shao, K. Shi, and K. Gong, "PET Image Denoising Based on 3D Denoising Diffusion Probabilistic Model: Evaluations on Total-Body Datasets," in *Medical Image Computing and Computer Assisted Intervention – MICCAI 2024*, vol. 15007, M. G. Linguraru, Q. Dou, A. Feragen, S. Giannarou, B. Glocker, K. Lekadir, and J. A. Schnabel, Eds. Cham: Springer Nature Switzerland, 2024, pp. 541–550.

[11] I. Kruzhilov, S. Kudin, L. Vetoshkin, E. Sokolova, and V. Kokh, "Whole-body PET image denoising for reduced acquisition time," *Frontiers in Medicine*, vol. 11, Sept. 2024, Art. no. 1415058, https://doi.org/10.3389/fmed.2024.1415058.

[12] M. Carles *et al.*, "Development and evaluation of two open-source nnU-Net models for automatic segmentation of lung tumors on PET and CT images with and without respiratory motion compensation," *European Radiology*, vol. 34, no. 10, pp. 6701–6711, Apr. 2024, https://doi.org/10.1007/s00330-024-10751-2.

[13] Z. Wang, A. C. Bovik, H. R. Sheikh, and E. P. Simoncelli, "Image quality assessment: from error visibility to structural similarity," *IEEE Transactions on Image Processing*, vol. 13, no. 4, pp. 600–612, Apr. 2004, https://doi.org/10.1109/TIP.2003.819861.

[14] K. Zuiderveld, "Contrast Limited Adaptive Histogram Equalization," in *Graphics Gems*, Elsevier, 1994, pp. 474–485.

[15] N. Otsu, "A Threshold Selection Method from Gray-Level Histograms," *IEEE Transactions on Systems, Man, and Cybernetics*, vol. 9, no. 1, pp. 62–66, Jan. 1979, https://doi.org/10.1109/TSMC.1979.4310076.

[16] T. Shepherd *et al.*, "Comparative Study With New Accuracy Metrics for Target Volume Contouring in PET Image Guided Radiation Therapy," *IEEE Transactions on Medical Imaging*, vol. 31, no. 11, pp. 2006–2024, Nov. 2012, https://doi.org/10.1109/TMI.2012.2202322.

[17] A. De Biase *et al.*, "Deep learning-based outcome prediction using PET/CT and automatically predicted probability maps of primary tumor in patients with oropharyngeal cancer," *Computer Methods and Programs in Biomedicine*, vol. 244, Feb. 2024, Art. no. 107939, https://doi.org/10.1016/j.cmpb.2023.107939.

[18] O. Ronneberger, P. Fischer, and T. Brox, "U-Net: Convolutional Networks for Biomedical Image Segmentation," in *Medical Image Computing and Computer-Assisted Intervention – MICCAI 2015*, vol. 9351, N. Navab, J. Hornegger, W. M. Wells, and A. F. Frangi, Eds. Cham: Springer International Publishing, 2015, pp. 234–241.

[19] Y. R. Habarnau and M. Namías, "A mirror-Unet architecture for PET/CT lesion segmentation." arXiv, Sept. 2023, https://doi.org/10.48550/arXiv.2309.13398.

[20] Ö. Çiçek, A. Abdulkadir, S. S. Lienkamp, T. Brox, and O. Ronneberger, "3D U-Net: Learning Dense Volumetric Segmentation from Sparse Annotation," in *Medical Image Computing and Computer-Assisted Intervention – MICCAI 2016*, vol. 9901, S. Ourselin, L. Joskowicz, M. R. Sabuncu, G. Unal, and W. Wells, Eds. Cham: Springer International Publishing, 2016, pp. 424–432.

[21] Z. Zhou, M. M. Rahman Siddiquee, N. Tajbakhsh, and J. Liang, "UNet++: A Nested U-Net Architecture for Medical Image Segmentation," in *Deep Learning in Medical Image Analysis and Multimodal Learning for Clinical Decision Support*, vol. 11045, D. Stoyanov, Z. Taylor, G. Carneiro, T. Syeda-Mahmood, A. Martel, L. Maier-Hein, J. M. R. S. Tavares, A. Bradley, J. P. Papa, V. Belagiannis, J. C. Nascimento, Z. Lu, S. Conjeti, M. Moradi, H. Greenspan, and A. Madabhushi, Eds. Cham: Springer International Publishing, 2018, pp. 3–11.

[22] F. Isensee, P. F. Jaeger, S. A. A. Kohl, J. Petersen, and K. H. Maier-Hein, "nnU-Net: a self-configuring method for deep learning-based biomedical image segmentation," *Nature Methods*, vol. 18, no. 2, pp. 203–211, Feb. 2021, https://doi.org/10.1038/s41592-020-01008-z.

[23] D. Xiang, B. Zhang, Y. Lu, and S. Deng, "Modality-Specific Segmentation Network for Lung Tumor Segmentation in PET-CT Images," *IEEE Journal of Biomedical and Health Informatics*, vol. 27, no. 3, pp. 1237–1248, Mar. 2023, https://doi.org/10.1109/JBHI.2022.3186275.

[24] A. Firouzian, M. D. Kelly, and J. M. Declerck, "Insight on automated lesion delineation methods for PET data," *EJNMMI Research*, vol. 4, no. 1, Dec. 2014, Art. no. 69, https://doi.org/10.1186/s13550-014-0069-8.

[25] S. Venkatesh *et al.*, "Multi-Annotator Consensus Network with Adaptive Preprocessing for Lung Nodule Segmentation: A Deep Learning Framework for Clinical Decision Support," *Engineering, Technology & Applied Science Research*, vol. 15, no. 6, pp. 29566–29573, Dec. 2025, https://doi.org/10.48084/etasr.12408.

[26] S. Lalitha and P. Nimmagadda, "VASC-Net: A Novel AI Framework Combining CNN Architectures with SVM for Lung Cancer Detection," *Engineering, Technology & Applied Science Research*, vol. 15, no. 6, pp. 29722–29730, Dec. 2025, https://doi.org/10.48084/etasr.12243.

[27] M. Xia *et al.*, "Anatomically and metabolically informed diffusion for unified denoising and segmentation in low-count PET imaging," *Medical Image Analysis*, vol. 107, Jan. 2026, Art. no. 103831, https://doi.org/10.1016/j.media.2025.103831.

[28] X. Lin *et al.*, "Intratumoral and peritumoral PET/CT-based radiomics for non-invasively and dynamically predicting immunotherapy response in NSCLC," *British Journal of Cancer*, vol. 132, no. 6, pp. 558–568, Apr. 2025, https://doi.org/10.1038/s41416-025-02948-z.

[29] P. Taheri and A. Golden, "A prognostic PET radiomic model for risk stratification in non-small cell lung cancer: integrating radiogenomics and clinical features to predict survival and uncover tumor biology insights," *Journal of Cancer Research and Clinical Oncology*, vol. 151, no. 6, June 2025, Art. no. 180, https://doi.org/10.1007/s00432-025-06232-8.

[30] G. M. Alshmrani, Q. Ni, R. Jiang, and N. Muhammed, "Hyper-Dense_Lung_Seg: Multimodal-Fusion-Based Modified U-Net for Lung Tumour Segmentation Using Multimodality of CT-PET Scans," *Diagnostics*, vol. 13, no. 22, Nov. 2023, Art. no. 3481, https://doi.org/10.3390/diagnostics13223481.

[31] V. Balaji, T.-A. Song, M. Malekzadeh, P. Heidari, and J. Dutta, "Artificial Intelligence for PET and SPECT Image Enhancement," *Journal of Nuclear Medicine*, vol. 65, no. 1, pp. 4–12, Jan. 2024, https://doi.org/10.2967/jnumed.122.265000.

[32] S. Gatidis and T. Kuestner, "A whole-body FDG-PET/CT dataset with manually annotated tumor lesions (FDG-PET-CT-Lesions)." The Cancer Imaging Archive, 2022, https://doi.org/10.7937/GKR0-XV29.

AUTHORS PROFILE

N. Shruthi received her M.Tech. in Software Engineering from Sri Jayachamarajendra College of Engineering, Mysuru (2015), and her B.E. in Information Science and Engineering from Maharaja Institute of Technology, Mysore (2011), under Visvesvaraya Technological University, Belagavi, India. She is currently an Assistant Professor in the Department of Information Science and Engineering at JSS Science and Technology University, Mysuru. She is a Life Member of MISTE and MIE. She has published numerous research papers in reputed international journals and conferences, and holds one innovation (utility) patent in the field of medical imaging and machine learning. Her research interests include image processing, machine learning, medical imaging, and intelligent systems.

N. Manju obtained his B.E. in Computer Science and Engineering from Sri Jayachamarajendra College of Engineering (SJCE), Mysuru, followed by an M.Tech in Computer Network Engineering from the National Institute of Engineering (NIE), Mysuru. He earned his Ph.D. from Visvesvaraya Technological University (VTU). He is currently serving as an Associate Professor in the Department of Information Science and Engineering at JSS Science and Technology University, Mysuru. He has published several research articles in peer-reviewed international journals and conferences, and also holds a patent to his credit. He has contributed to the academic community as a reviewer for various international journals and conferences. He has served as a Technical Program Committee (TPC) member and has chaired sessions at multiple international conferences. Additionally, he has been a jury member for several academic and technical events. He has organized numerous Workshops, Faculty Development Programs (FDPs), and Invited Talks, and has served as an external member on the Board of Examinations (BoE) and Board of Studies (BoS) for various institutions. He is a Life Member of ISTE. His research interests include Machine Learning, Computational Intelligence, Image Processing, and Computer Networks.